High-pressure spectroscopic investigation of multiferroic Ni_{3}TeO_{6}

Kenneth R. O'Neal, Amanda J. Clune, Nathan C. Harms, Sang-Wook Cheong, Junjie Yang, Zhenxian Liu, Turan Birol, and Janice L. Musfeldt

High pressure spectroscopic investigation of multiferroic Ni_3TeO_6

Kenneth R. O'Neal,[1] Amanda J. Clune,[1] Nathan C. Harms,[1] Sang-Wook

Cheong,[2] Junjie Yang,[3] Zhenxian Liu,[4] Turan Birol,[5] and Janice L. Musfeldt[1,6]

[1]*Department of Chemistry, University of Tennessee, Knoxville, Tennessee 37996, USA*

[2]*Rutgers Center for Emergent Materials and Department of Physics and Astronomy,*

Rutgers University, Piscataway, New Jersey 08854, USA

[3]*Department of Physics, Central Michigan University, Mount Pleasant, MI 48859*

[4]*Department of Civil and Environmental Engineering,*

The George Washington University, Washington DC 20052, USA

[5]*Chemical Engineering and Materials Science,*

University of Minnesota, Minneapolis, MN 55455

[6]*Department of Physics and Astronomy,*

University of Tennessee, Knoxville, Tennessee 37996, USA

(Dated: October 15, 2018)

Abstract

We combined diamond anvil cell techniques, infrared and Raman spectroscopies, and lattice dynamics calculations to explore the high pressure properties of multiferroic Ni_3TeO_6. Using a frequency trend analysis, we trace a subtle decrease in compressibility near 4 GPa to a minimum in the O-Ni2-O bond angle. This unique behavior emanates from the proximity of the Ni2 center in the Ni3-Ni2-Ni1-Te chain to a flexible pocket that is intrinsic to the crystal structure. At the same time, predicted trends in the super-exchange pathways are consistent with greater antiferromagnetic character under compression, in line with both phase stability calculations and direct susceptibility measurements. These findings highlight opportunities for local structure control of corrundum-like materials.

*Address correspondence to musfeldt@utk.edu.

INTRODUCTION

Multiferroics are fascinating materials where ferroelectric and magnetic orders coexist, and spatial inversion and time reversal symmetries are simultaneously broken.[1-5] As a consequence, their properties tend to be controllable (at least to some degree) with external stimuli like voltage, magnetic field, pressure, and light. These materials are also potential platforms for the development of ultra-low-power multi-state memory, switching devices, and novel computing architectures.[6-8] While theoretical work has pointed to a number of exciting opportunities for strain- and pressure-control of ferroic properties,[9-11] the area has been under-explored from an experimental point of view.[12,13] Corundum-like materials such as Cr_2O_3 and $MnTiO_3$[14,15] are particularly attractive because the structural motif includes empty cavities. The latter may be important for enhanced pressure or strain control of ferroic ordering.

Ni_3TeO_6 is another material with which we can examine these issues. This system crystallizes in a polar space group ($R3$) and consists of Ni3-Ni2-Ni1-Te chains along the c direction [Fig. 1].[16] There are three unique Ni environments, so we distinguish them as labeled in Fig. 1 (a). Each Ni is an $S = 1$ center, whereas the Te ions are non-magnetic. Ni_3TeO_6 is a collinear antiferromagnet below T_N=53 K.[17] The spins are arranged in a ↑ ↑ ↓; ↓ ↓ ↑ pattern [Fig. 1 (d)].[18,19] Magnetic field drives a non-hysteretic spin-flop transition at 9 T as well as a metamagnetic transition near 52 T - each accompanied by changes in polarization and spin pattern.[18-21] While temperature and magnetic field effects have been extensively studied,[18-22] the role of other external stimuli (such as pressure or light) is much less investigated. In particular, the presence of large cavities in the crystal structure may provide enhanced sensitivity to pressure or strain.

In this work, we bring together diamond anvil techniques, infrared and Raman spectroscopies, magnetic property measurements, and density functional theory-based lattice dynamics calculations to investigate the high pressure response of Ni_3TeO_6. While overall crystal symmetry is preserved up to (and beyond) 10 GPa, an analysis of vibrational mode trends uncovers reduced compressibility near 4 GPa that we trace to a rather surprising tendency in a particular local lattice distortion. Specifically, the O-Ni2-O bond angles nearest to the large octahedrally-shaped cavity decrease upon compression, reach a minimum near 4 GPa, and increase again at higher pressures. In order to develop magnetostructural correlations, we also analyze trends in the calculated super-exchange pathways. We find enhanced antiferromagnetic character under compression - in excellent agreement with the relative energetic stability of various candidate spin states as well as complementary susceptibility measurements that reveal how the Néel transition temperature
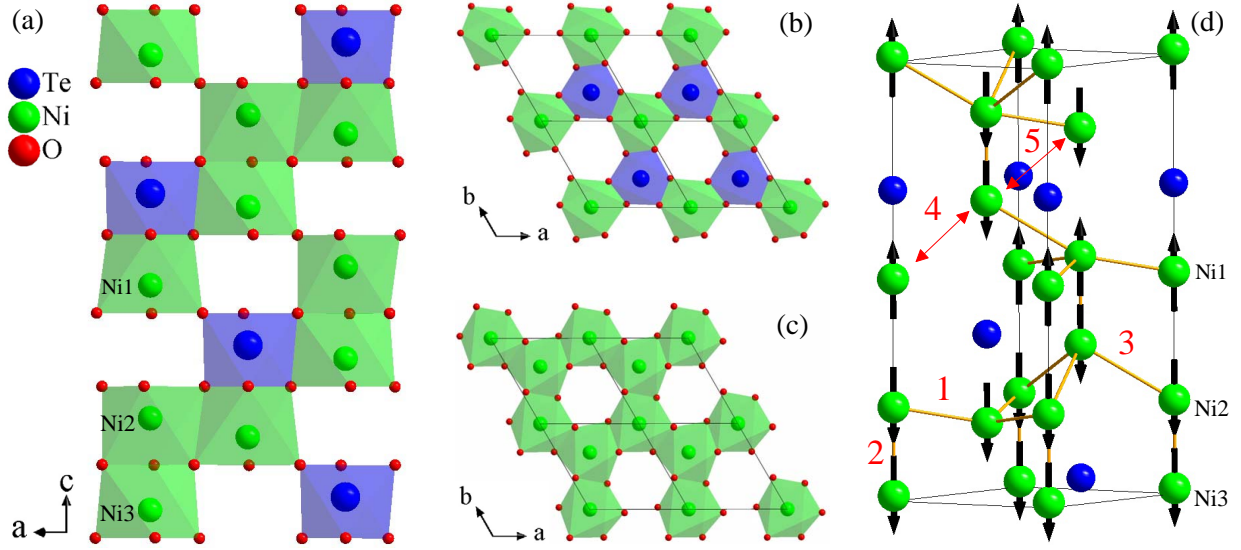
2

FIG. 1. (a) 300 K crystal structure of Ni_3TeO_6 viewed (a) perpendicular to and (b,c) along the Ni-Ni-Ni-Te chain direction.[16] The (b) Te-Ni3 and (c) Ni1-Ni2 planes are offset such that large empty cavities are formed. These cavities are surrounded by each type of NiO_6 and TeO_6 environment. (d) Schematic view of the spin pattern and various superexchange interactions in Ni_3TeO_6.

(T_N) increases under pressure. More broadly, empty cavities like the octahedrally-shaped pocket in Ni_3TeO_6 concentrates stress, suggesting that local structure may be more easily controlled when in close proximity to these vacancies. As an example, we discuss how the large frequency shifts that emanate from these effects might be advantageous for pumping experiments.

METHODS

Ni_3TeO_6 was synthesized using flux techniques as described previously.[18] Polycrystalline sample was loaded into a diamond anvil cell with vacuum grease or KBr as a pressure medium for infrared measurements and neat for Raman scattering. The matrix acts as a pressure medium and, at the same time, provides control of the optical density. Spectroscopic data were collected using several different diamond anvil cells equipped with either type IIa or low fluorescence diamonds with culet sizes ranging from 300 - 500 μm. Annealed ruby balls along with direct fluorescence measurements of the $R1$ ruby line were used to determine pressure inside the cell.[23] Infrared spectra were taken using a Fourier transform infrared spectrometer equipped with a liquid helium cooled bolometer. 4 cm^{-1} resolution was employed. Raman spectra were measured using an 1800 g/mm grating and a 532 nm laser with power below 10 μW to prevent sample degradation, integrated

up to 120 s, and averaged as needed. Although we collected both infrared and Raman spectra in the 0 - 20 GPa range, we focus on the 0 - 10 GPa region here. No pressure cycling effects were observed. Standard peak fitting procedures were employed to reveal frequency trends. Magnetic susceptibility measurements were carried out using a vibrating sample magnetometer (Quantum Design, PPMS) at a magnetic field of 0.1 T. Self-clamped piston cylinder cells made with CuBe were used as pressure cells for magnetic susceptibility measurements under high pressure. Daphne 7373 oil was chosen as the pressure transmitting medium. The applied pressure was calibrated by measuring the superconducting transition temperature of a tiny lead piece.[24]

First-principles density functional theory calculations were performed to predict crystal structures and phonon frequencies at increasing pressures. The disagreement between the theoretical and experimental frequencies is in the 3-8% range, and in certain plots a constant is added to theoretical values in order to better match the experimental values and make the pressure trends easier to compare. We used the projector-augmented wave method as implemented in VASP and the PBE exchange correlation functional.[25–27] The plane wave cutoff energy is set to 500 eV, and an $8 \times 8 \times 8$ Monkhorst Pack grid is used for the primitive cell that contains one formula unit. In order to properly reproduce the interactions on the partially filled d shell of the Ni ion, we set an on-site Coulomb repulsion U to 5 eV and employed ferromagnetic ordering. Lowering U, using a different spin arrangement, or employing a different generalized gradient approximation changes the quantitative results (such as the critical pressure discussed below) significantly, but the overall qualitative trends in the structure are similar. Magnetic energies are calculated and compared in a 60 atom supercell and reported per formula unit.

RESULTS AND DISCUSSION

Figure 2 displays the infrared and Raman spectra of Ni_3TeO_6 under compression. While some features are difficult to resolve, the overall number and position of the peaks are in excellent agreement with prior work[19,22] as well as our updated lattice dynamics calculations, so we adopt the previously assigned symmetries and displacement patterns. As a reminder, a symmetry analysis of the $R3$ space group yields 9 doubly-degenerate E symmetry and 9 singly-degenerate A symmetry modes. Both are infrared- and Raman-active.[28] In this framework, modes below 350 cm^{-1} correspond to motion of the Te and/or Ni centers, whereas higher frequency modes involve mostly O displacements. All modes display traditional hardening under compression, with frequency shifts that are surprisingly large for an oxide. The sizable frequency shifts (ranging from 1.2 to 5.5
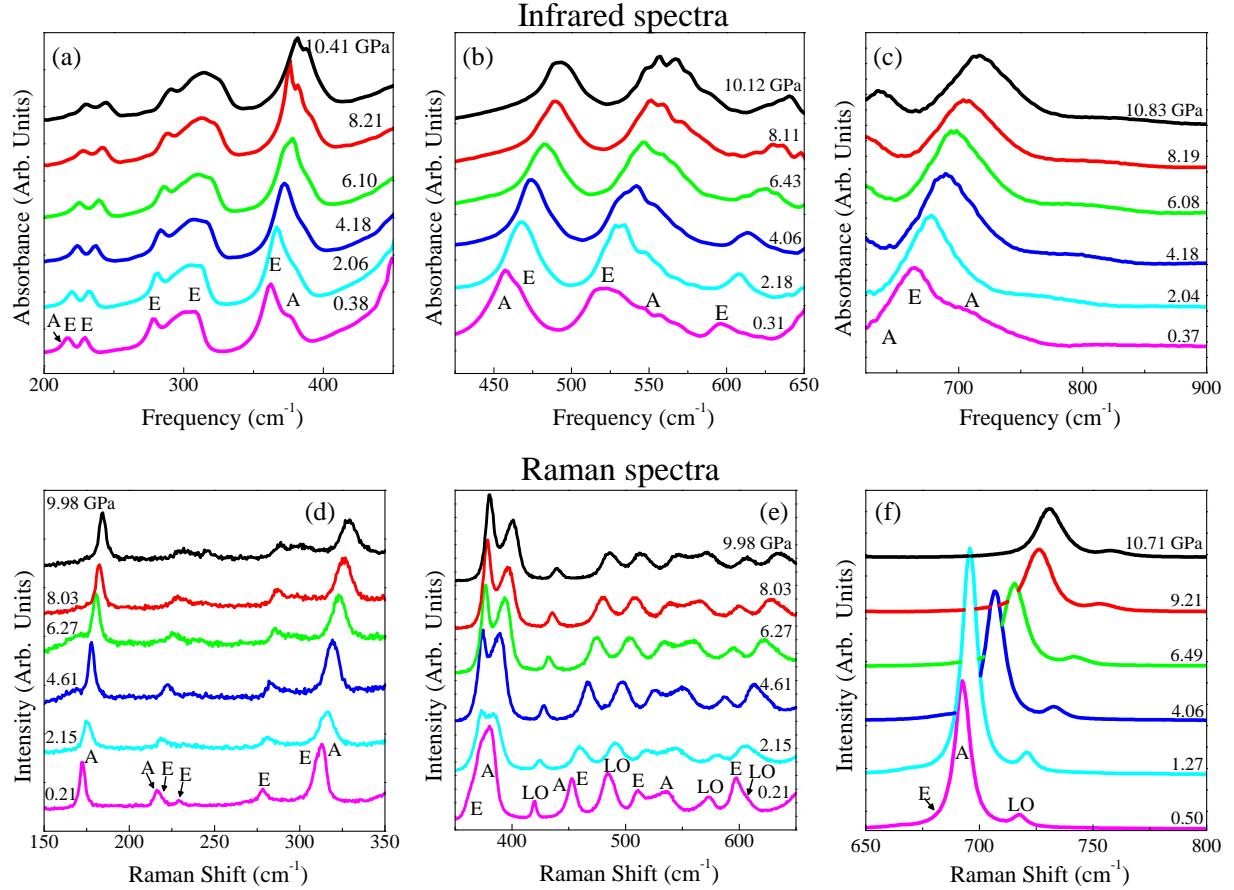
Infrared spectra

Raman spectra

FIG. 2. Representative (a-c) infrared and (d-f) Raman spectra of Ni_3TeO_6 at the indicated pressures. Mode symmetries are labeled based on previous single crystal assignments.[19,22] All polarizations are observed due to the polycrystalline nature of the sample.

cm^{-1}/GPa depending on the mode) derive from the presence of open cavities in the corundum-like structure.[29,30] There is no splitting (and only limited broadening) within our resolution - an indication that, while there may be local structure modifications, the overall crystal symmetry signified by the $R3$ space group is preserved.[31]

Figure 3 (a-c) displays the frequency of three representative vibrational modes along with the results of our lattice dynamics calculations as a function of pressure. The infrared and Raman branches of the 228, 278, and 541 cm^{-1} modes track each other quite well. In other cases, there are small splittings (up to 10 cm^{-1}) between the infrared and Raman branches (Supplemental Information). Examination of these trends reveals a subtle change in the frequency vs. pressure curves near 4 GPa. The effect is most noticeable in the low frequency modes that involve Ni and/or Te motion [Fig. 3 (a,b)]. The higher frequency modes related to O displacements are insensitive to these effects [Fig. 3 (c)]. Derivatives of the frequency vs. pressure data better characterize

the subtle change in compressibility near 4 GPa. Focusing on the calculated trends, we find that $\partial\omega/\partial P$ of the low frequency modes such as those at 228 and 278 cm^{-1} decrease sharply near 4 GPa [Fig. 3 (d, e)] whereas the response of the higher frequency modes (for instance at 541 cm^{-1}) change smoothly across this range [Fig. 3 (f)].[31] The experimental trends are in general overall agreement with theory, albeit with significant scattering due to experimental error bars. Fine tuning the theoretical parameters such as the on-site Coulomb repulsion U may give better agreement with experiment, but we did not attempt to do this here.
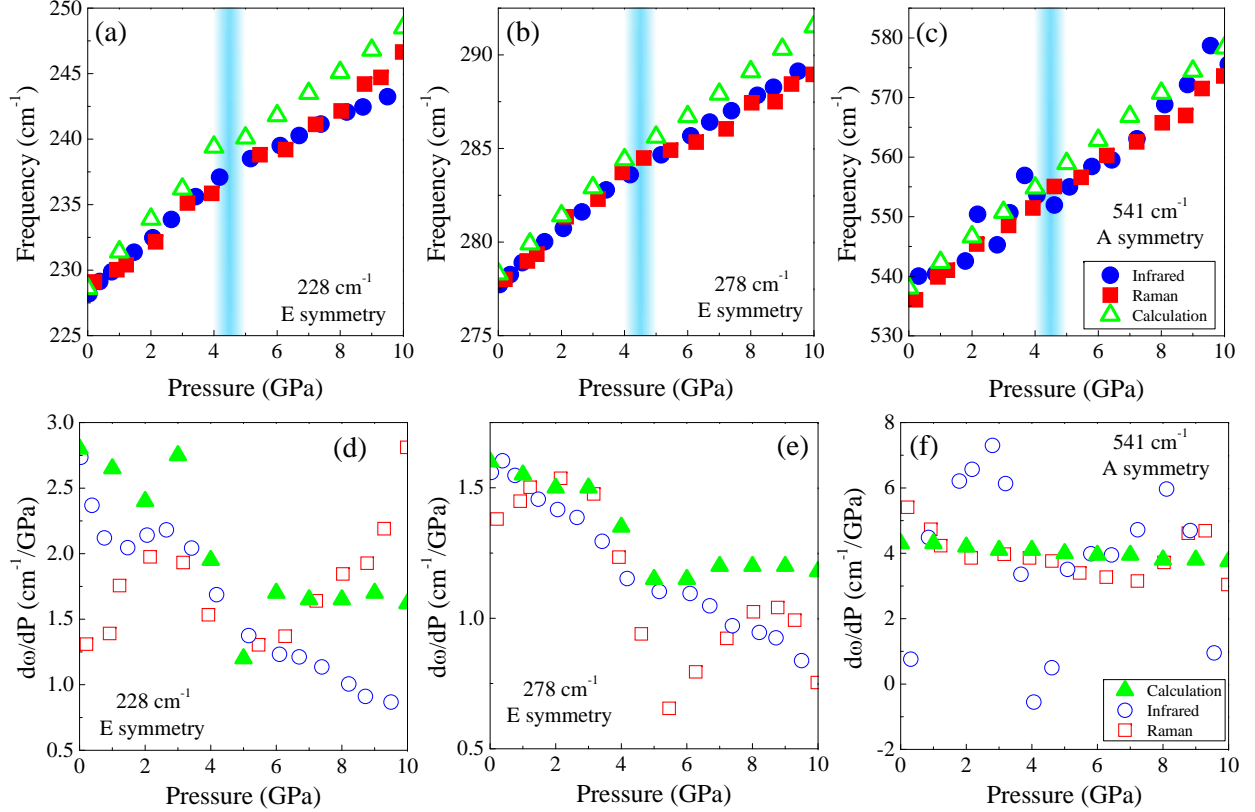

FIG. 3. (a-c) Infrared, Raman, and theoretical mode frequencies vs pressure for selected modes of Ni$_3$TeO$_6$. According to our mode assignments, the displacement pattern of the 228 cm^{-1} mode is ab plane motion of the Ni and Te centers, that of the 278 cm^{-1} mode contains Ni and Te motion along c, and that of the 541 cm^{-1} modes is NiO$_6$ octahedral contraction and rotation.[31] The vertical blue line denotes the compressibility crossover near 4 GPa. (d-f) Derivatives of the frequency vs pressure data for this set of vibrational modes. Experimental data were smoothed to reduce scattering and emphasize the trends.

The correlation between theoretical and experimental trends in Fig. 3 suggests that the calculated high pressure structures hold the key to understanding the subtle change in compressibility

near 4 GPa. Moreover, the $R3$ space group is maintained across this entire pressure range, so the difference must be related to local lattice distortions. We therefore extracted bond lengths and angles from the relaxed structures of Ni_3TeO_6 predicted at each pressure and analyzed the trends. According to our calculations, the bond distances decrease gradually under compression. There are no sharp changes or reversals. The bond angles are different. While the majority change systematically under pressure, one of the angles has a very unusual trend. Specifically, the O-Ni2-O bond angle decreases upon compression, reaches a minimum near 4 GPa, and increases again at higher pressures [Fig. 4 (a)]. This bond angle reversal is the only structural signature of what may be happening near 4 GPa. Like other corrundum-like materials, Ni_3TeO_6 has octahedrally-shaped cavities embedded in the crystal structure. These cavities are surrounded by the three unique Ni environments as well as the Te environment [Fig. 1 (b)]. While compressing the cavity is a logical primary volume reduction pathway, the bond lengths and angles (and the modes that probe them) are not equally affected. Instead, they depend upon proximity to the empty cavity. Our analysis reveals that the the set of oxygen centers involved in the O-Ni2-O angles are in fact vertices of the empty cavity in the Ni-Ni-Ni-Te chain. It is these centers, with their close proximity to the empty cavity, that engage in bond angle trend reversal under pressure.

Since magnetoelastic coupling in Ni_3TeO_6 is strong[20,21] and magnetic ordering temperatures are generally quite sensitive to pressure[32–34], it is useful to consider how compression is likely to modify the superexchange pathways between magnetic centers. As a reminder, there are five unique superexchange angles between the $S = 1$ Ni^{2+} ions [Fig. 1 (d)].[21,35] Figure 4 (b) summarizes how these angles are predicted to change under compression. These data were extracted from relaxed structures at different pressures - obtained from our first principles calculations. At ambient pressure conditions, two of the superexchange angles are close to $90°$ and therefore support mostly ferromagnetic interactions. The others are larger and are antiferromagnetic in nature.[17] Focusing on the behavior of the two angles that are close to $90°$ [Fig. 4 (b)], we see that both are predicted to diverge with increasing pressure. This is consistent with an overall decrease in ferromagnetic tendencies. We therefore find that antiferromagnetic exchange strengthens under compression. As a result, T_N should increase with pressure. There may even be a change in microscopic spin arrangement.[36] In order to test these predictions, we calculated the relative stability of several different candidate spin states with respect to the energy of the collinear antiferromagnetic state of Ni_3TeO_6. As shown in Fig. 4 (c), the antiferromagnetic state is stabilized compared to the ferromagnetic state under compression. As a further test of these predictions, we measured magnetic
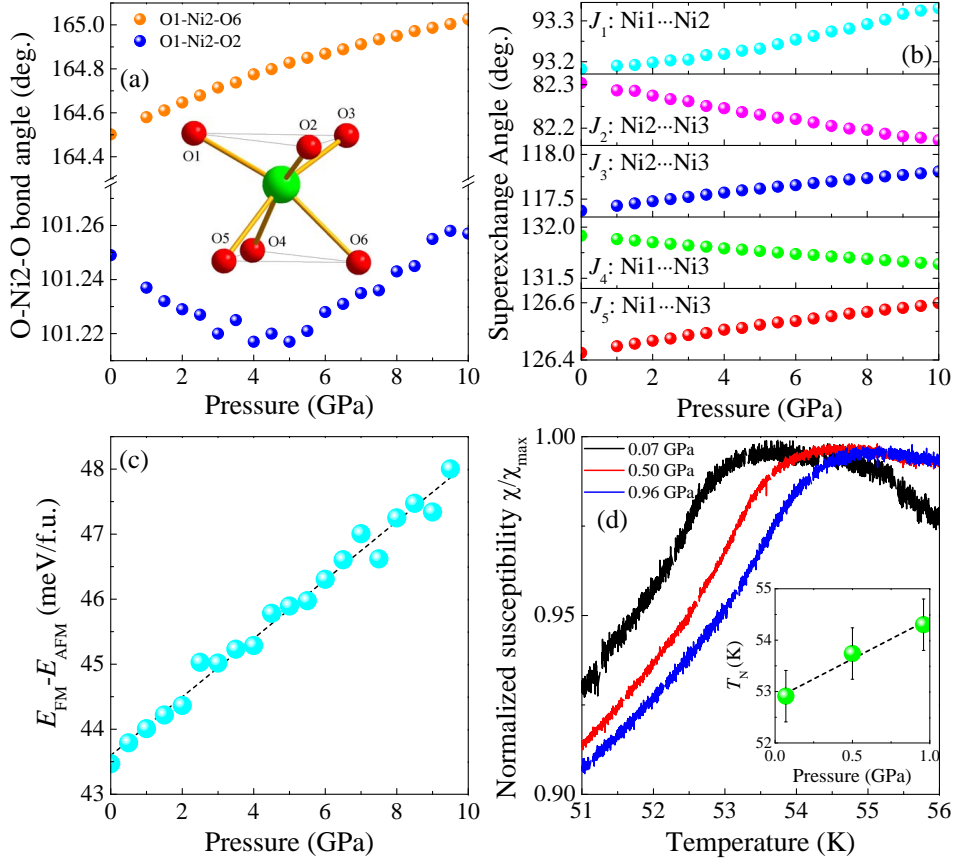
FIG. 4. (a) Representative O-Ni2-O bond angles vs. pressure highlighting the unique behavior of the O1-Ni2-O2 angle. The inset displays the Ni2 environment. Here, the O1-3 atoms face the empty cavity. (b) Predicted Ni-O-Ni superexchange angles vs. pressure. (c) Calculated energy difference between the ferromagnetic (FM) and antiferromagnetic (AFM) spin states. (d) Normalized susceptibility of Ni_3TeO_6 experimentally measured at different pressures. The inset shows that T_N increases with pressure.

susceptibility under pressure. We find that, at least up to 1 GPa, T_N increases with pressure [Fig. 4 (d)] - thus verifying these predictions. Interestingly, antiferromagnetic interactions in Cr_2O_3 also strengthen under pressure as evidenced by the behavior of T_N.[14]

Compression is also likely to impact other properties of Ni_3TeO_6. Electrical polarization is among the most important. Strong magnetoelectric coupling in this system is such that decreasing the antiferromagnetic character (for instance, by applying magnetic field to cant the spins) reduces the electric polarization.[18] The same mechanism may work in the opposite direction. In other words, we know that pressure increases antiferromagnetic tendencies in Ni_3TeO_6, so it is reasonable to suspect that electric polarization might be enhanced under compression. Direct measurements of polarization under pressure or compressive strain along with x-ray diffraction to reveal the loss

of the inversion center are obviously needed to confirm this strategy. Similar tendencies in which pressure enhances ferroelectricity are found in other multiferroics like $TbMnO_3$ and the RMn_2O_5 (R=Tb, Dy, Ho) family of materials.[37,38]

Finally, we point out that pressure control of mode position may also offer important opportunities in combination with laser pumping experiments. The idea is that by pumping a particular mode, one can trigger properties or even access new dynamical phases. Once a decision is made as to which mode to pump, one traditionally searches for a laser to match this energy. This work suggests an alternate approach. Corrundum-like materials like Ni_3TeO_6 clearly have very large frequency shifts under pressure. We find $\partial\omega/\partial P$ on the order of 1 - 5 cm^{-1}/GPa in Ni_3TeO_6 - depending on the mode. Thus, one can imagine tuning a phonon into resonance with an infrared pump laser via compression in a diamond anvil cell rather than tuning the laser to match the mode energy. This strategy could open interesting opportunities for the discovery of new properties and phases in ferroic materials.

CONCLUSION

To summarize, we combined diamond anvil cell techniques, infrared and Raman spectroscopies, and density functional theory-based lattice dynamics calculations to explore the properties of Ni_3TeO_6 under pressure. Analysis of vibrational mode trends reveals a decrease in compressibility near 4 GPa that can be traced to a rather surprising tendency in a specific local lattice distortion. Specifically, the O-Ni2-O angles (which are nearest to the empty cavity) decrease under pressure, reach a minimum near 4 GPa, and rise again with increasing compression. Moreover, pressure-induced changes in the superexchange pathways are consistent with enhanced antiferromagnetic character - in excellent agreement with predictions of thermodynamic stability as well as direct magnetic property measurements that demonstrate higher T_N under compression. Thus we attribute the reduced compressibility near 4 GPa as due to a competition between increasing antiferromagnetic interactions and volume effects. These findings lay the groundwork for future high pressure studies of Ni_3TeO_6 and highlight potential opportunities for control of local structure in the vicinity of large cavities in multifunctional materials.

SUPPORTING INFORMATION

Supporting information is available including spectra up to 20 GPa, frequency trends and derivatives for all modes, and predicted unit cell parameters, bond lengths, and bond angles.

[1] S.-W. W. Cheong and M. Mostovoy. Nat. Mater. **6**, 13 (2007).

[2] M. Fiebig, T. Lottermoser, D. Meier, and M. Trassin. Nat. Rev. Mater. **1**, 16046 (2016).

[3] Y. Tokura, S. Seki, and N. Nagaosa. Reports Prog. Phys. **77**, 076501 (2014).

[4] N. A. Spaldin, S.-W. Cheong, and R. Ramesh. Phys. Today **63**, 38 (2010).

[5] D. Khomskii. Physics (College. Park. Md). **2**, 20 (2009).

[6] J. Kaur, J. Kaur, J. Shah, R. K. Kotnala, V. Gupta, and K. C. Verma. Adv. Mater. Lett. **3**, 371 (2012).

[7] Y. Wang, G. L. Pascut, B. Gao, T. A. Tyson, K. Haule, V. Kiryukhin, and S.-W. Cheong. Sci. Rep. **5**, 12268 (2015).

[8] S. Mittal. ACM J. Emerg. Technol. Comput. Syst. **13**, 29 (2016).

[9] P. K. Das, N. Mandal, and A. Arya. J. Appl. Phys. **122**, 225107 (2017).

[10] D. G. Schlom, L. Q. Chen, C. J. Fennie, V. Gopalan, D. A. Muller, X. Pan, R. Ramesh, and R. Uecker. MRS Bull. **39**, 118 (2014).

[11] E. Cockayne and K. M. Rabe. J. Phys. Chem. Solids **61**, 305 (2000).

[12] E. Gilioli and L. Ehm. IUCrJ **1**, 590 (2014).

[13] N. Poudel, M. Gooch, B. Lorenz, C.-W. Chu, J. Kim, and S.-W. Cheong. IEEE Trans. Magn. **52**, 2501204 (2016).

[14] Y. Kota, Y. Yoshimori, H. Imamura, and T. Kimura. Appl. Phys. Lett. **110**, 042902 (2017).

[15] F. Zhu, X. Wu, and S. Qin. Solid State Commun. **152**, 984 (2012).

[16] R. Becker and H. Berger. Acta Crystallogr. E **62**, i222 (2006).

[17] I. Živković, K. Prša, O. Zaharko, and H. Berger. J. Phys. Condens. Matter **22**, 056002 (2010).

[18] Y. S. Oh, S. Artyukhin, J. J. Yang, V. Zapf, J. W. Kim, D. Vanderbilt, and S.-W. Cheong. Nat. Commun. **5**, 3201 (2014).

[19] M. O. Yokosuk, A. Al-Wahish, S. Artyukhin, K. R. O'Neal, D. Mazumdar, P. Chen, J. Yang, Y. S. Oh, S. A. McGill, K. Haule, S.-W. Cheong, D. Vanderbilt, and J. L. Musfeldt. Phys. Rev. Lett. **117**, 147402 (2016).

[20] M. O. Yokosuk, S. Artyukhin, A. Al-Wahish, X. Wang, J. Yang, Z. Li, S.-W. Cheong, D. Vanderbilt, and J. L. Musfeldt. Phys. Rev. B **92**, 144305 (2015).

[21] J. W. Kim, S. Artyukhin, E. D. Mun, M. Jaime, N. Harrison, A. Hansen, J. J. Yang, Y. S. Oh, D. Vanderbilt, V. S. Zapf, and S.-W. Cheong. Phys. Rev. Lett. **115**, 137201 (2015).

[22] S. Skiadopoulou, F. Borodavka, C. Kadlec, F. Kadlec, M. Retuerto, Z. Deng, M. Greenblatt, and S. Kamba. Phys. Rev. B **95**, 184435 (2017).

[23] H. K. Mao, P. M. Bell, J. W. Shaner, and D. J. Steinberg. J. Appl. Phys. **49**, 3276 (1978).

[24] B. Bireckoven and J. Wittig. J. Phys. E. **21**, 841 (1988).

[25] G. Kresse and J. Furthmüller. Phys. Rev. B **54**, 11169 (1996).

[26] G. Kresse and J. Hafner. Phys. Rev. B **47**, 558 (1993).

[27] J. P. Perdew, A. Ruzsinszky, G. I. Csonka, O. A. Vydrov, G. E. Scuseria, L. A. Constantin, X. Zhou, and K. Burke. Phys. Rev. Lett. **100**, 136406 (2008).

[28] H. T. Stokes, D. M. Hatch, and J. D. Wells. Phys. Rev. B **43**, 11010 (1991).

[29] S.-H. Shim, T. S. Duffy, R. Jeanloz, C.-S. Yoo, and V. Iota. Phys. Rev. B **69**, 144107 (2004).

[30] X. Wu, S. Qin, and L. Dubrovinsky. Geosci. Front. **2**, 107 (2011).

[31] See the Supplemental Information for more details.

[32] J. G. Dasilva and J. S. Miller. Inorg. Chem. **52**, 1418 (2013).

[33] P. H. M. van Loosdrecht, J. Zeman, G. Martinez, G. Dhalenne, and A. Revcolevschi. Phys. Rev. Lett. **78**, 487 (1997).

[34] P. A. Quintero, D. Rajan, M. K. Peprah, T. V. Brinzari, R. S. Fishman, D. R. Talham, and M. W. Meisel. Phys. Rev. B **91**, 014439 (2015).

[35] F. Wu, E. Kan, C. Tian, and M. H. Whangbo. Inorg. Chem. **49**, 7545 (2010).

[36] K. R. O'Neal, J. H. Lee, M.-S. Kim, J. L. Manson, Z. Liu, R. S. Fishman, and J. L. Musfeldt. npj Quantum Mater. **2**, 65 (2017).

[37] T. Aoyama, K. Yamauchi, A. Iyama, S. Picozzi, K. Shimizu, and T. Kimura. Nat. Commun. **5**, 4927 (2014).

[38] C. R. dela Cruz, B. Lorenz, Y. Y. Sun, Y. Wang, S. Park, S. W. Cheong, M. M. Gospodinov, and C. W. Chu. Phys. Rev. B **76**, 174106 (2007).